Entropy Drives Integrin αIIbβ3:Echistatin Binding—Evidence from Surface Plasmon Resonance Spectroscopy[†]

Roy R. Hantgan,* Mary C. Stahle, and David A. Horita

Department of Biochemistry, Wake Forest University School of Medicine, Medical Center Boulevard, Winston-Salem, North Carolina 27157-1016

Received September 13, 2007; Revised Manuscript Received December 6, 2007

ABSTRACT: This investigation examined the molecular mechanisms that enable the αIIbβ3 integrin to bind efficiently, tightly, and selectively to echistatin, an RGD disintegrin. We used surface plasmon resonance spectroscopy to measure the rate, extent, and stability of complexes formed between micellar αIIbβ3 and recombinant echistatin (rEch) mutants, immobilized on the surface of a biosensor chip. αIIbβ3 bound readily and tightly to wild-type RGD-rEch and RGDF-rEch but not to RGA-rEch or AGD-rEch, demonstrating that both of those charged moieties contribute to integrin recognition. van't Hoff analysis of the temperature dependence of the RGD-rEch K_d data yielded an unfavorable enthalpy change, $\Delta H^\circ = 14 \pm 3$ kcal/mol, offset by a favorable entropy term, $T\Delta S^\circ = 23 \pm 3$ kcal/mol. Eyring analysis of the temperature dependence of the kinetic parameters yielded $\Delta H_a^{\circ\ddagger} = 9 \pm 2$ kcal/mol and $T\Delta S_a^{\circ\ddagger} = -4 \pm 2$ kcal/mol, indicating that a substantial activation enthalpy barrier and a smaller activation entropy hinder assembly of the encounter complex. Thus, equilibrium thermodynamic data demonstrate that entropy is the dominant factor stabilizing integrin:echistatin binding, while transition-state thermodynamic parameters indicate that the rate of complex formation is enthalpy-limited. When electrostatic contacts are the major source of receptor:ligand stability, theory and experiment indicate that entropy-favorable ion-pair desolvation often provides the driving force for molecular recognition.

Regulated ligand recognition by the αIIbβ3 integrin, present at high density on the surface of human blood platelets, is central to normal hemostasis and aberrant in cardiovascular disease (*1–3*). Despite immersion in a saturating fibrinogen concentration, these adhesive receptors only bind their primary physiological ligand following a cascade of intracellular signals (*4–6*). Conformational changes in the ectodomain of αIIbβ3, initiated allosterically through uncoupling of negative effectors at its distant cytoplasmic segments, enable fibrinogen binding in a process whose molecular mechanisms are still emerging (*7–11*). Crystal structures are available for the extracellular domains of both β3 integrins: αvβ3, resting (*12*) and with a cyclic RGD-peptide bound (*13*), and αIIbβ3, crystallized in the presence of pharmaceutical integrin antagonists (*14*). However, structural details of interactions of αIIbβ3 with adhesive proteins can only be gleaned from images obtained by electron microcopy (*15–19*) or atomic force microscopy (*17, 20*). Thus, many intriguing questions remain about the dynamic regulation of integrin structure and function (*21–24*).

Snake venom disintegrins can provide unique insights because they recognize their target integrins under resting cellular conditions that exclude larger and more abundant adhesive proteins from the cryptic ligand-binding pocket of αIIbβ3 (*25, 26*). For example, echistatin, the prototypical RGD-disintegrin, blocks fibrin(ogen)-dependent platelet adhesiveness at near stoichiometric concentrations (*27–29*). Echistatin binding to platelets and to purified integrins is itself blocked by pharmaceutical integrin antagonists acting as competitive inhibitors (*29, 30*). Moreover, we and others have also shown that echistatin shares with pharmaceutical GpIIb/IIIa inhibitors the ability to shift a conformational equilibrium from a resting to a primed, possibly prothrombotic, state (*29, 31*). Thus, echistatin provides a powerful platform for studying the relationship between integrin structure and ligand affinity, a multifaceted problem whose resolution can enhance our fundamental understanding of protein:protein interactions, as well as promote the development of safer, more effective cardiovascular disease drugs.

We recently combined site-directed mutagenesis, biophysical probes of integrin conformation, and molecular modeling to demonstrate that echistatin binding perturbs the conformation of αIIbβ3 (*32*) in a process that is mediated by electrostatic interactions between the RGD loop of the

[†] This work was supported by Grant-in-Aid 0555527U from the American Heart Association, Mid-Atlantic Affiliate (to R.R.H.), the Dubie H. Holleman Cancer & Heart Research Fund (to R.R.H.), Grant AI064609 from the National Institutes of Health (to D.A.H.), and Institutional Development Grant 2006-IDG-1004 from the North Carolina Biotechnology Center (to R.R.H.).

* To whom correspondence should be addressed. Telephone: 336-716-4675. Fax: 336-716-7671. E-mail: rhantgan@wfubmc.edu.

[1] Abbreviations: rEch, recombinant echistatin; RGD-rEch, recombinant full-length echistatin (1–49) M28L; AGD-rEch, rEch (1–49) R24A M28L; RGA-rEch, rEch (1–49) D26A M28L; RGDF-rEch, rEch (1–49) D27F M28L; HSCM-OG, pH 7.4 buffer containing 0.13 mol/L NaCl, 0.01 mol/L HEPES, 0.03 mol/L *n*-octyl-β-D-glucopyranoside, and 0.001 mol/L $CaCl_2$/0.001 mol/L $MgCl_2$; HS-OG, pH 7.4 buffer containing 0.13 mol/L NaCl, 0.01 mol/L HEPES, 0.03 mol/L *n*-octyl-β-D-glucopyranoside; RU, response units; SPR, surface plasmon resonance; ITC, isothermal titration calorimetry.

10.1021/bi701877a CCC: $40.75
Published on Web 02/01/2008

disintegrin and charged moieties at the αIIb/β3 subunit interface (*33*). In this study, we have used surface plasmon resonance (SPR) spectroscopy[1] (*34, 35*) to measure the rate and extent of complex formation between αIIbβ3 and echistatin as a function of the temperature, enabling the calculation of both equilibrium and transition-state thermodynamic parameters for this fundamental molecular recognition process. We will present evidence that the entropy-favorable desolvation of ion pairs promotes the assembly and stability of the αIIbβ3:echistatin complex.

EXPERIMENTAL PROCEDURES

αIIbβ3 Purification. Milligram quantities of highly purified αIIbβ3 were isolated from outdated human blood platelets (Blood Bank, North Carolina Baptist Hospital, Winston-Salem, NC) as previously described (*36, 37*). Monodisperse αIIbβ3 was obtained by size-exclusion chromatography at 4 °C on a 1.6 × 40 cm column of Sephacryl S-300 equilibrated in a pH 7.4 buffer containing 0.13 mol/L NaCl, 0.01 mol/L *N*-2-hydroxyethylpiperazine-*N*′-2-ethanesulfonic acid (HEPES), 0.03 mol/L *n*-octyl-β-D-glucopyranoside, and 0.001 mol/L $CaCl_2$/0.001 mol/L $MgCl_2$ (HSCM-OG). Peak fractions were then concentrated in an Amicon pressure concentrator with a PLHK cellulose membrane, at a 100 000 Da retention limit. Concentrations of the αIIbβ3 integrin were determined from its UV absorbance using an extinction coefficient at 280 nm of 1.21 mL mg^{-1} cm^{-1}, determined by carefully calibrated amino acid analyses as previously described (*36*). Extensive biophysical characterizations have yielded molecular weight, sedimentation coefficient, and diffusion coefficient data, demonstrating that this micellar integrin preparation contains the heterodimeric αIIbβ3 complex with little or no contamination from higher order oligomers (*37, 38*).

Expression and Purification of Echistatin Variants. Recombinant full-length echistatin, rEch (1–49) M28L (RGD-rEch), and variants with point mutations in its integrin-recognition loop: rEch (1–49) R24A M28L (AGD-rEch), rEch (1–49) D26A M28L (RGA-rEch), and rEch (1–49) D27F M28L (RGDF-rEch) were prepared using cloning, site-directed mutagenesis, expression, and purification protocols previously described (*32, 33*).

Biosensor Preparations. The dextran surfaces of CM5 or CM3 biosensor chips (Biacore, Inc., Piscataway, NJ), both sample and reference flow chambers, were activated for amine coupling by reaction with 1-ethyl-3-(3-dimethylaminopropyl)carbodiimide and *N*-hydroxysuccinimide using automated algorithms in a Biacore T100 instrument. Sequential aliquots of a recombinant echistatin variant, diluted to 5–50 μg/mL in 0.1 M sodium acetate buffer at pH 5.0 were delivered to the sample flow chamber in an automated process designed to achieve an immobilization density in the range of 40–140 response units (RU). Because a 1000 RU signal typically results from immobilization of a protein at a density of 1 ng/mm^2 on a 100 nm thick dextran layer (*34*), this corresponds to a surface concentration in the range of 0.1–0.3 mM echistatin ligand. In addition, an aliquot of running buffer, 0.01 M HEPES and 0.15 M NaCl at pH 7.4 containing 0.05% surfactant P20, was delivered to the activated reference channel. An excess of ethanolamine was then delivered to block any remaining active groups on both channels, followed by equilibration with running buffer. Each echistatin-immobilized biosensor chip was subsequently equilibrated with HSCM-OG buffer and used for up to three experiments, each with 8−12 cycles of integrin binding, dissociation, and regeneration.

We assessed the stability of echistatin immobilized on a biosensor chip by examining data obtained with a CM3 chip with covalently coupled RGDF that was first used to measure the temperature dependence of integrin binding at 15, 25, and 35 °C. Thus, this chip was used for a total of 36 cycles at integrin concentrations ranging from 50 to 2500 nM. In a subsequent experiment, data were collected at 25 °C at integrin concentrations ranging from 200 to 1000 nM. A comparison of the RU versus integrin concentration profiles yielded a signal that was ∼80% of the initial value even after 36 cycles; similar kinetic parameters were also obtained.

SPR Spectroscopy. Measurements of rate and extent of complex formation between immobilized echistatin variants and the αIIbβ3 integrin were performed in a Biacore T100 instrument by monitoring the changes in RU at the biosensor surface. Signals from both the reference and sample channels were collected at a rate of 10 Hz, and the data were reported as the difference, thus correcting for changes in the refractive index because of solvent mismatches, as well as nonspecific integrin binding to the ligand-free surface. Reagents were maintained at 25.0 ± 0.1 °C in the sample compartment; data were collected at temperatures ranging from 15 to 40 °C with control to ±0.01 °C in the analysis chamber.

Initially, two start-up cycles were performed at each temperature, during which HSCM-OG buffer was delivered to the sample and reference channels, followed by a two-step regeneration cycle. Next, during the binding steps, increasing concentrations of αIIbβ3 integrin (0–3000 nM) were delivered at a flow rate of 30 μL/min for 700 s; dissociation of the echistatin:integrin complexes was then monitored for 1600 s as HSCM-OG buffer flowed over the biosensor surface at 30 μL/min. Residual bound integrin was displaced by a two-step regeneration cycle: 20 mM ethylenediaminetetraacetic acid (EDTA) in HEPES-buffered saline at pH 7.4 with 30 mM octyl glucoside (HS-OG) for 180 s and then 5 M NaCl in HS-OG for 180 s. The biosensor was then equilibrated for 300 s with HSCM-OG prior to delivery of the next integrin aliquot.

Data Analysis: Kinetics. The sensorgram responses, the difference in RU versus time between sample and reference channels at each integrin concentration, were further corrected by subtracting the time-dependent profiles obtained with a buffer blank. These buffer corrections were typically in the range from −3 to +7 RU, corresponding to 2–4% of the maximum signal changes observed during integrin binding. These doubly corrected signals (*39*) were then fit globally by nonlinear regression (Biacore evaluation software) to a reversible bimolecular interaction model (*34*) to determine the forward (k_a, L mol^{-1} s^{-1}) and reverse (k_d, s^{-1}) rate constants for integrin:echistatin binding

$$\alpha\mathrm{IIb}\beta3_{o} \xrightarrow{k_t} \alpha\mathrm{IIb}\beta3 + \mathrm{rEch} \underset{k_d}{\overset{k_a}{\rightleftharpoons}} \alpha\mathrm{IIb}\beta3{:}\mathrm{rEch} \qquad (1)$$

Because reaction rates in the flow chamber may be limited by the rate of analyte diffusion from bulk solution to the vicinity of the biosensor surface, the fitting procedure also

yielded the mass-transfer rate constant, k_t (RU L mol^{-1} s^{-1}) (*40, 41*). Selected data sets were also analyzed with software (Scrubber 2, BioLogic Software Pty Ltd., Campbell, Australia) that enabled a direct comparison of fits with and without a mass-transfer term. The quality of the fits were judged by the residuals, as well as the signal/noise ratio, defined as the $\langle RU \rangle / \sqrt{\chi^2}$.

Data Analysis: Equilibrium Thermodynamics. The equilibrium dissociation constant (K_d, L/mol) was then determined from the ratio of the resultant kinetic parameters

$$K_d = k_d/k_a \quad (2)$$

K_d data obtained as a function of the temperature were analyzed using the integrated van't Hoff equation

$$\ln K_d = \Delta H^\circ/RT - \Delta S^\circ/R \quad (3)$$

Changes in enthalpy (ΔH°, kcal/mol) and entropy (ΔS°, cal K^{-1} mol^{-1}) were calculated from the slope and intercept, respectively, obtained by linear regression (Sigma Plot, Jandel Scientific). The uncertainties in ΔH° and ΔS° were computed from the standard errors of the fitted parameters. All data are reported at the reference temperature, T°, of 298.15 K; R is the ideal gas constant.

Data Analysis: Transition-State Thermodynamics. Kinetic parameters obtained as a function of temperature were analyzed using the transition-state theory according to the Eyring equation to obtain the activation enthalpy ($\Delta H^{\circ\ddagger}$) and entropy ($\Delta S^{\circ\ddagger}$)

$$\ln kh/k_b T = \Delta H^{\circ\ddagger}/RT + \Delta S^{\circ\ddagger}/R \quad (4)$$

Here, k is the rate constant, h is Planck's constant, and k_b is Boltzmann's constant. Linear regression performed with temperature-dependent k_a or k_d data yielded the thermodynamic activation parameters and their experimental uncertainties for assembly of the integrin:echistatin transition state, starting from reactants or products, respectively.

RESULTS

SPR Analysis of Integrin Binding to Recombinant Echistatin. SPR data demonstrate that integrin αIIbβ3, isolated in a resting conformation in octyl glucoside micelles (*37*), exhibits temperature-dependent, bimolecular binding kinetics upon exposure to recombinant echistatin immobilized on the surface of a biosensor chip. The resultant kinetic data, as well as equilibrium and transition-state thermodynamic parameters, provide new insights into the molecular recognition mechanisms that enable an RGD disintegrin to bind efficiently, tightly, and reversibly, primarily through electrostatic interactions, to a receptor with a central role in hemostasis and cardiovascular disease.

Kinetic Parameters. RGD-rEch. Figure 1 presents RU versus time profiles obtained as a function of the αIIbβ3 concentration and temperature for the interaction of integrin with wild-type RGD-rEch. All traces have been corrected for the small signal changes observed when buffer, rather than integrin, was delivered to each biosensor. Data at each temperature were analyzed globally in terms of a 1:1 binding model characterized by a forward rate constant, k_a, and a reverse rate constant, k_d. For example, data obtained at 25 °C exhibited $k_a = 1.167 \pm 0.002 \times 10^3$ L mol^{-1} s^{-1} and $k_d = 2.993 \pm 0.002 \times 10^{-4}$ s^{-1}. The solid lines in the left middle panel of Figure 1, obtained with those fitted parameters, provide an accurate description of the data, as evidenced by their close correspondence with the experimental points (signal/noise ratio of 180:1) and the reasonably tight distribution of the residuals presented below the kinetic traces. The ratio of the reverse and forward rate constants yielded $K_d = 2.56 \times 10^{-7}$ mol/L for the αIIbβ3:RGD-rEch complex at 25 °C. This dissociation constant was derived from SPR data obtained at integrin concentrations ranging from 0.06 to 8 times K_d, i.e., from substoichiometric to nearly saturating.

Temperature-Dependent Binding. Analysis of integrin:RGD-rEch binding data obtained at both lower and higher temperatures with a 1:1 binding model demonstrated that the forward rate constant, k_a, increased approximately 3-fold from 15 to 35 °C, while k_d varied by less than 10% (Figure 1). There are some small, systematic deviations between the fitted lines and experimental points, most evident at high integrin concentrations and elevated temperatures. However, the overall quality of the fit based on a 1:1 binding model is quite reasonable, judged by the distributions of the residuals and the signal/noise ratios, which ranged from 300:1 at 15 °C to 100:1 at 35 °C. The fit quality was somewhat diminished at 40 °C, where thermal aggregation of the bound integrin (*32*) may have contributed to the 70:1 signal/noise ratio.

Validation of Kinetic Model. Simulations indicate that under these conditions, characterized by relatively slow on-rates, there is no detectable influence of mass transport on the kinetic parameters so that the k_t terms are not significant. This point was further explored by examining selected data sets with software (Scrubber 2, BioLogic Software Pty Ltd., Campbell, Australia) to compare fits with and without a mass-transfer term; those rate constants agreed within 5%, providing further confirmation that mass transport does not have a significant impact on the rate constants that we have determined.

Specificity of Binding. Recognizing the need to demonstrate specificity, we included the potent integrin antagonist, tirofiban, at a saturating concentration (100 μM) in selected samples containing midrange αIIbβ3 concentrations (480–600 nM) and repeated the kinetic profiles at each temperature. On the basis of our experience with this inhibitor in fluid-phase steady-state and kinetic studies, we anticipated that tirofiban would fully disrupt integrin binding (*29*). Indeed, a consistent reduction in the binding signal resulted, as evidenced by the open black symbols in each panel in Figure 1. The mechanism for these negative traces in the presence of tirofiban is unclear; however, the magnitude of this effect became smaller at increasing temperatures.

RGA- and AGD-rEch. Micellar αIIbβ3 exhibited minimal interactions with RGA-rEch, an inactive mutant, which lacks the conserved aspartate (*25*) that coordinates the MIDAS cation of the integrin (*33*). For example, delivery of 600 nM αIIbβ3 to immobilized RGA-rEch yielded a small negative signal change (open red symbols in the left-middle panel of Figure 1). Similar negative RU versus time profiles were obtained with integrin concentrations ranging from 200 to 2000 nM (data not shown). αIIbβ3 delivery to immobilized AGD-rEch yielded more pronounced negative signal changes, as illustrated by data obtained with 600 nM receptor (open blue symbols in the left-middle panel of Figure 1A). Minimal

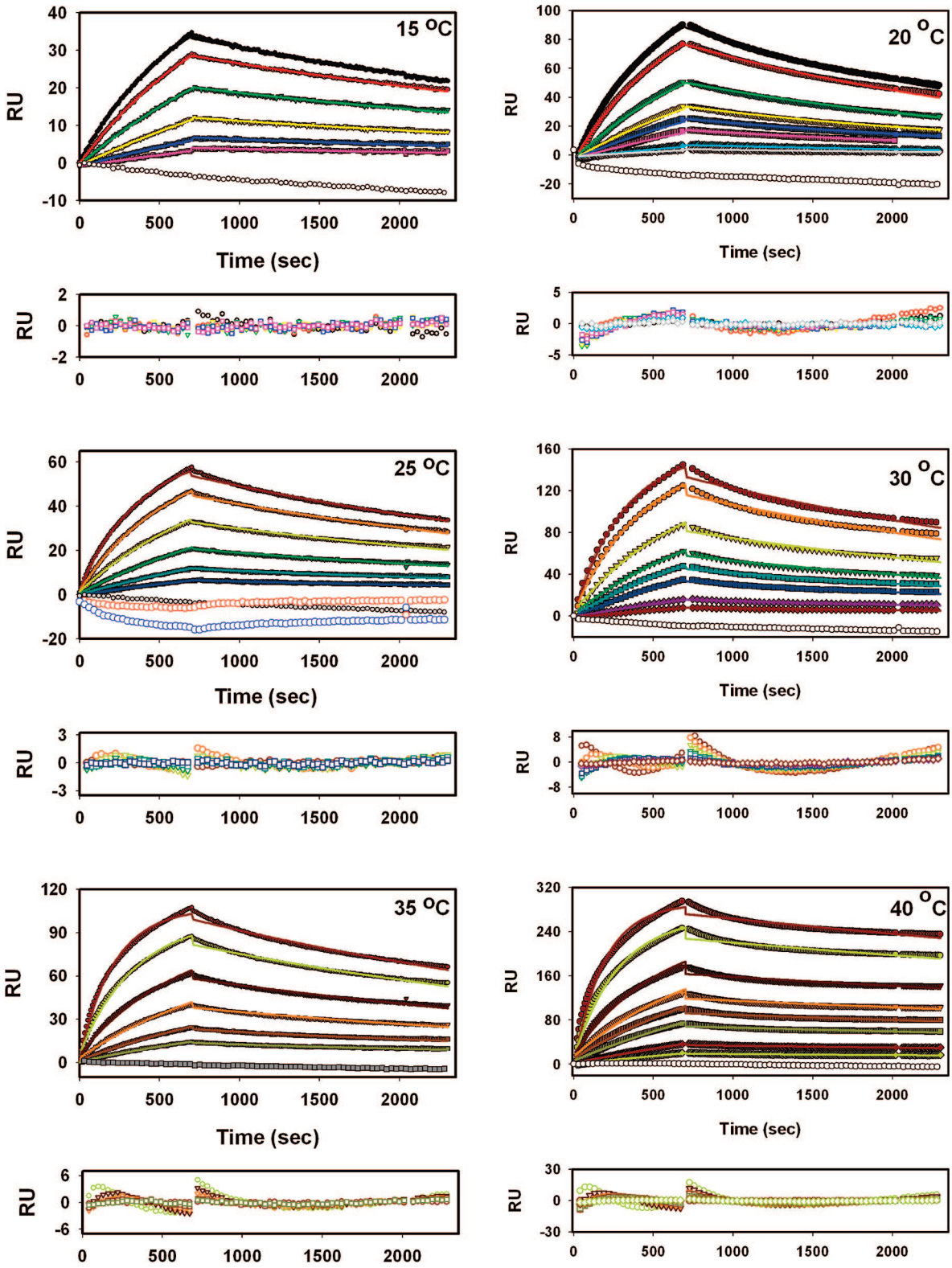

FIGURE 1: Kinetics of αIIbβ3 binding to immobilized echistatin measured by SPR spectroscopy. Integrin binding profiles: The left panel presents integrin binding data obtained as a function of temperature (15, 25, and 35 °C) with RGD-echistatin immobilized on a CM5 biosensor chip in a Biacore T100 instrument. Increasing concentrations of αIIbβ3 (solid symbols, from the bottom to the top: 74, 150, 301, 599, 1201, and 2001 nM) were delivered to the surface during the 700 s binding period. The right panel presents data obtained in a separate experiment: 20, 30, and 40 °C; αIIbβ3 concentrations: 52, 105, 251, 404, 603, 1000, 2001, and 3002 nM. In all experiments, dissociation was monitored during the subsequent 1600 s as buffer was delivered to the chip. All traces have been corrected for the small RU changes observed with buffer alone in the binding and dissociation steps. The surface was regenerated with 20 mM EDTA and then 5 M NaCl prior to the next integrin addition. Fitting functions and residual plots: The solid lines in each panel were obtained by fitting the data to a 1:1 reversible binding model (eq 1) using Biacore software as described in the Experimental Procedures. Residual plots are presented below each data panel at ±5% of the scale of the corresponding RU versus time figures, except for 40 °C data, which are scaled at ±9%. Nonspecific binding controls: Open black symbols/left panel show data obtained with 482 nM αIIbβ3 plus 100 μM tirofiban, an integrin antagonist, and the open black symbols/right panel show data obtained with 603 nM αIIbβ3 plus 100 μM tirofiban. Echistatin mutants: Left middle panel, 25 °C, open red symbols show data obtained with 600 nM αIIbβ3 delivered to immobilized RGA-rEch, and the open blue symbols show data obtained with 600 nM αIIbβ3 delivered to immobilized AGD-rEch.

integrin binding to AGD-rEch was anticipated on the basis of its 25-fold weaker integrin-perturbation activity profile compared to RGD-rEch (*33*). Moreover, simulated titration profiles (ExPasy Proteomics Tools) indicate that AGD-rEch will have a net charge near zero at pH 7.4, one unit lower than RGD-rEch, so that unfavorable electrostatic interactions between immobilized AGD-rEch and the strongly negatively charged integrin may explain these downward RU profiles.

Taken together, data obtained with these charged-to-alanine mutants demonstrate the requirement for both the positive charge on Arg-24 of echistatin and the negative charge on Asp-26 for optimal integrin recognition.

RGDF-rEch. Analysis of duplicate SPR experiments obtained with αIIbβ3 binding to immobilized RGDF-rEch at 25 °C (Supplementary Figure 1 in the Supporting Information) yielded $k_a = 1.68 \pm 0.20 \times 10^3$ L mol^{-1} s^{-1}, $k_d = 3.99 \pm 0.35 \times 10^{-4}$ s^{-1}, and $K_d = 240 \pm 49$ nM for RGDF-rEch, parameters that were statistically indistinguishable ($p > 0.08$) with those obtained in duplicate profiles with RGD-rEch, $k_a = 1.21 \pm 0.07 \times 10^3$ L mol^{-1} s^{-1}, $k_d = 3.52 \pm 0.75 \times 10^{-4}$ s^{-1}, and $K_d = 289 \pm 45$ nM. These dissociation constants are comparable to the K_d values in the 400–800 nM range that we recently reported for micellar αIIbβ3 binding to Oregon Green-labeled RGDW-rEch as determined by fluorescence anisotropy measurements (*29, 33*).

Additional experiments were performed with RGDF-rEch at temperatures ranging from 15 to 40 °C, as illustrated in Supplementary Figure 1 in the Supporting Information. However, analysis of these profiles with a 1:1 binding model was hampered by a signal/noise ratio that ranged from 80:1 at 15 °C to 30:1 at 40 °C, i.e., a fit quality consistently lower than with the RGD-rEch data. While improved fits could be obtained with a more complex model, such as a heterogeneous ligand or heterogeneous analyte model, both of those approaches required three additional fitted parameters, i.e., the association and dissociation rate constants for the second species and its binding capacity. Because both of those models precluded subsequent thermodynamic analysis in terms of a two-state system, we did not pursue further characterization of the RGDF-rEch data.

Equilibrium Thermodynamics. Dissociation constants for integrin:RGD-echistatin complexes were calculated from the ratio of the reverse to forward rate constants, $K_d = k_d/k_a$. The resultant equilibrium constants were analyzed using the integrated van't Hoff equation (eq 3 in the Experimental Procedures), to obtain the data presented in Figure 2, a plot of ln K_d versus $1/T$. Linear regression yielded the following parameters for assembly of the αIIbβ3:echistatin complex at 25 °C: $\Delta H° = 14.0 \pm 2.7$ kcal/mol and $\Delta S° = 76.6 \pm 9.1$ cal K^{-1} mol^{-1}; applying the Gibb's equation yielded $\Delta G° = -8.9 \pm 1.7$ kcal/mol. Thus, the overall thermodynamic stability of this integrin:disintegrin complex comes from an entropy/enthalpy balance, in which a favorable $T\Delta S$ term outweighs the unfavorable ΔH, as will be explored in the Discussion.

Recognizing the power of isothermal titration calorimetry (ITC) (*42*) to provide a direct measure of the reaction enthalpy for integrin:rEch binding, we performed a series of exploratory experiments with a MicroCal VPC ITC instrument (kindly made available by Dr. Karen Buchmueller, Department of Chemistry, Wake Forest University). However, the high background heat obtained in blank titrations with RGD-rEch and RGDF-rEch diluted into buffered octyl glucoside (*43*) precluded obtaining reliable data with the integrin concentrations available, ~4 μM.

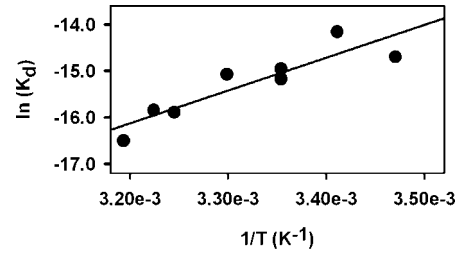

FIGURE 2: van't Hoff analysis of the temperature dependence of the equilibrium dissociation constants for integrin:echistatin complexes. Data are presented as the natural logarithm of the dissociation constant, K_d versus $1/T$ (inverse of the Kelvin temperature) for αIIbβ3:RGD-rEch complexes (●). In each case, K_d was calculated from the ratio of the kinetic constants, k_d/k_a, obtained from data such as that presented in Figure 1. The solid line was obtained by linear regression. The enthalpy ($\Delta H°$) and entropy ($\Delta S°$) changes for formation of an αIIbβ3:rEch complex were calculated from the slope and intercept of that regression line, respectively, according to eq 3.

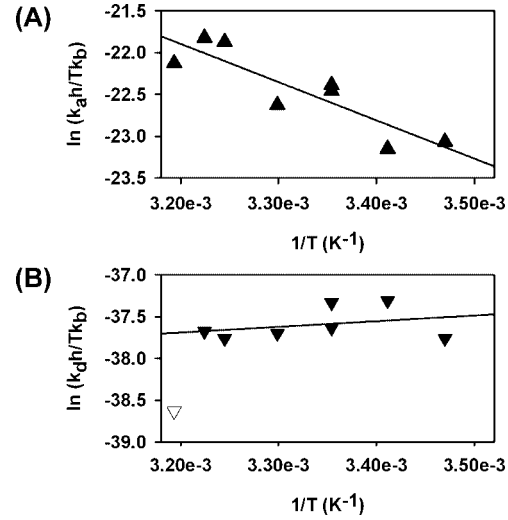

FIGURE 3: Eyring analysis of the temperature dependence of the rate constants for the formation and dissociation of integrin:echistatin complexes. (A) Data are presented as the natural logarithm of the association rate constant, k_a, divided by the Kelvin temperature and scaled by the ratio of Planck's constant, h, to Boltzmann's constant, k_b, versus $1/T$ for αIIbβ3:RGD-rEch complexes (▲). The activation enthalpy ($\Delta H_a^{\circ\ddagger}$) and entropy ($\Delta S_a^{\circ\ddagger}$) were calculated from the slope and intercept, respectively, of the solid line that was obtained by linear regression according to eq 4. (B) Analogous procedures were followed for the dissociation rate constant, k_d, data (▼) to obtain $\Delta H_d^{\circ\ddagger}$ and $\Delta S_d^{\circ\ddagger}$. Note that the k_d value obtained at 40 °C, denoted by the white downward triangle, was omitted from the fit.

Transition-State Thermodynamics. Analysis of the temperature dependence of the SPR-determined forward rate constant, k_a, for RGD-rEch in terms of the Eyring equation (eq 4 in the Experimental Procedures) yielded Figure 3A. Linear regression yielded the following activation parameters for the formation of the integrin:disintegrin transition-state complex from its reactants: $\Delta H_a^{\circ\ddagger} = 9.1 \pm 2.0$ kcal/mol, $\Delta S_a^{\circ\ddagger} = -14.4 \pm 6.6$ cal K^{-1} mol^{-1}, and $\Delta G_a^{\circ\ddagger} = 13.4 \pm 3.1$ kcal/mol. While the activation entropy is less well-determined, because of errors inherent in the large extrapolation to $1/T = 0$, the $T\Delta S_a^{\circ\ddagger}$ term only accounts for ~30% of $\Delta G_a^{\circ\ddagger}$. These observations demonstrate that an unfavorable

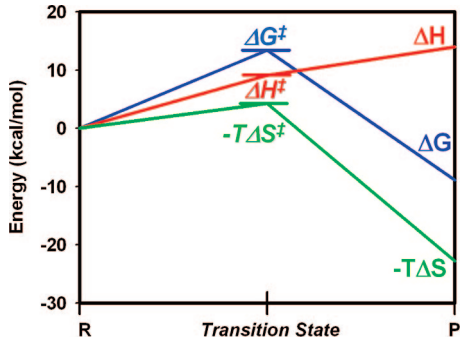

FIGURE 4: Free-energy profile for integrin αIIbβ3:echistatin interactions. This figure depicts the changes in free energy, ΔG, starting with reactants and proceeding through the encounter complex on the pathway to the formation of a thermodynamically stable integrin:ligand complex. Also shown are the competing changes in enthalpy, ΔH, and entropy, expressed as $-T\Delta S$, that contribute to $\Delta G \sim -9$ kcal/mol.

activation enthalpy is the dominant term hindering the formation of the αIIbβ3:echistatin transition-state complex from the reactants.

Recognizing the limitations inherent in applying transition-state theory to kinetic data, including that obtained with biosensors (*44, 45*), we also analyzed these data in terms of the empirical Arrhenius treatment. The resultant activation energy, $E_a = 9.7 \pm 2.0$ kcal/mol, exhibited the expected agreement with $\Delta H_a^{\circ\ddagger}$. The pre-exponential factor, 23.3 ± 3.3, was comparable to the universal frequency factor, 29.5, at 298 K. While this approach underscores the uncertainty in the activation entropy determined by the transition-state theory (*44*), it reinforces the concept of an enthalpic barrier to the formation of the encounter complex.

Applying the Eyring formalism to the k_d data for RGD-rEch produced Figure 3B and the following activation parameters for the formation of the integrin:disintegrin transition-state complex from its products: $\Delta H_d^{\circ\ddagger} = -1.3 \pm 1.9$ kcal/mol, $\Delta S_d^{\circ\ddagger} = -79.2 \pm 6.3$ cal K^{-1} mol^{-1}, and $\Delta G_d^{\circ\ddagger} = 22.3 \pm 1.8$ kcal/mol. Note that, in this case, k_d at 40 °C appeared as an outlier, most likely because of thermal aggregation; therefore, it was omitted from this linear regression. Overall, these observations suggest that an unfavorable activation, *entropy*, is the major barrier to assembly of the transition state from the product of the reaction, the thermodynamically stable integrin:disintegrin complex.

Reaction Coordinate Diagram. The combination of equilibrium and transition-state thermodynamic parameters derived from the temperature dependence of the binding and kinetic parameters for αIIbβ3:echistatin complexes enables the construction of the reaction coordinate diagram presented in Figure 4. Our data demonstrate that traversing the path from reactants to products requires overcoming a ~13 kcal/mol free-energy barrier in a process that is opposed by an enthalpic penalty, ~9 kcal/mol, at each step. Conversely, the entropy landscape is considerably more favorable because the relatively small entropic barrier (−4 kcal/mol) is offset by the substantial entropy gain of $T\Delta S$, ~23 kcal/mol, upon complex formation.

DISCUSSION

The principal result of this investigation is that integrin:echistatin binding is an entropy-driven phenomenon. Equilibrium thermodynamic data obtained in this study by SPR spectroscopy indicate that echistatin binding by the αIIbβ3 integrin is quite energetically favorable, characterized by $\Delta G^\circ = -8.9$ kcal/mol. Stability comes from a favorable entropic term, $T\Delta S^\circ = 22.8$ kcal/mol, partly offset by an unfavorable enthalpy change, $\Delta H^\circ = 14.0$ kcal/mol. These observations are intriguing because our SPR data with wild-type RGD-rEch and its mutants confirm that the formation of the αIIbβ3:rEch complex is critically dependent upon electrostatic interactions, primarily the ion pair formed between an aspartate on the RGD loop of echistatin and a divalent cation in the MIDAS site of αIIbβ3 (*33, 46*). Secondary stabilization is provided by an arginine:asparate salt bridge. In addition, the effects of introducing a nonpolar residue adjacent to the RGD site were rather modest (*28, 32, 33, 46*). While our SPR data yielded similar kinetic parameters for αIIbβ3 binding to immobilized wild-type echistatin and RGDF-rEch at 25 °C, kinetic traces obtained at elevated temperatures with the mutant did suggest some effects of the introduced hydrophobic residue, perhaps attributable to ligand-induced changes in integrin conformation or oligomerization (*32, 33*).

Thermodynamics of Receptor:Drug Binding. We also observed that the thermodynamic stability of the integrin αIIbβ3:echistatin complex is comparable to many receptor:drug interactions ($\Delta G^\circ = -9.5 \pm 2.1$ kcal/mol) (*47, 48*). Interestingly, Gilli et al. graphically demonstrated a pattern of an unfavorable enthalpy change compensated by increased entropy in $\sim^1/_3$ of those intermolecular associations (*47*). Because the snake venom disintegrins, echistatin and barbourin, are prototypes of the widely used antiplatelet drugs tirofiban (*49*) and eptifibatide (*50*), this observation may be more than coincidental. Because the drug design process involves optimization of hydrophobic and polar interactions while minimizing configurational entropic penalties (*51, 52*), it is challenging to parse their individual contributions from that data.

Entropy-favorable protein:protein and protein:ligand interactions are often associated with the desolvation of large expanses of *nonpolar* surface areas (*53*). Likewise, burying hydrophobic solutes results in a negative change in heat capacity, ΔC_p, whereas smaller, positive changes in ΔC_p are found with polar molecules (*54, 55*). Surveying a large number of biological interactions, Stites determined that $\Delta C_p = -80 \pm 48$ cal K^{-1} mol^{-1} for protein–protein interactions and -107 ± 74 cal K^{-1} mol^{-1} for protein−peptide binding (*55*). Our data, characterized by a linear van't Hoff plot, indicate that, within experimental error, $\Delta C_p = 0$ for integrin:echistatin binding. Hence, we scoured the literature in an effort to resolve the paradox presented by the entropy/enthalpy compensation effects that we observed for assembly of the integrin:echistatin complex from its strongly charged partners.

Ion Pairing Thermodynamics. In W. Kauzmann's classic 1959 monograph (*56*), often cited as the first description of the hydrophobic effect (*57*), he pointed out that Born's electrostatic theory predicts that salt-bridge formation in proteins is driven by a favorable desolvation entropy term and opposed by enthalpy. A recent comprehensive analysis of the thermodynamics of ion-pair formation with inorganic salts demonstrates that these interactions are often driven by a favorable desolvation entropy, which offsets a positive enthalpy change (*58*). The contributions of electrostatics to

protein stability has taken on new currency because theorists seeking to understand hyperthermostable proteins have shown by molecular dynamics that the strength of a salt bridge is remarkably invariant from 25 to 100 °C (*59*). However, ab initio computations indicate that ion-pair formation in proteins, characterized by a balance between a substantial desolvation energy penalty and favorable electrostatics, often provide less net stability than hydrophobic interactions (*60*). Conversely, theoretical considerations indicate that the stability of ion pairs in proteins strongly depends upon the local dielectric constant (*61, 62*).

Enthalpy/Entropy Compensation. Surveying experimental data on comparable systems, we note that ITC demonstrated how a pattern of uniformly positive entropy changes and a mix of favorable and unfavorable enthalpy changes contributes to the overall favorable free energy of divalent cation binding to synthetic peptides containing γ-carboxyglutamic acid residues (*63*). Calorimetric and structural data from a mutational analysis of protein antigen:antibody complexes also support the concept that positive entropy changes linked to desolvation of ion pairs plays a significant role in the stability of protein:ligand interactions (*64*). Thermodynamic data demonstrate a pattern of enthalpy/entropy compensation in binding negatively charged peptide ligands to a SH2 domain construct (*65*) and phosphotyrosine peptides to Src SH2 (*66*), as well as with zwitterionic active-site inhibitors binding to thrombin (*67*). However, the association of nonpolar reactants can also exhibit a favorable entropic component because of desolvation of hydrophobic surfaces, as evidenced by SPR and ITC data on the assembly of a native-like structure from complementing fragments of calbinin D_{9k} (*68*). Likewise, SPR and ITC data show that entropy drives complex formation between the immune system proteins LILRB1 and MHCI, an interface that involves both polar and nonpolar contacts (*69*). Conversely, cAMP binding to protein kinase A is dominated by a strongly favorable enthalpy change and opposed by a smaller entropic component (*70*).

Thermodynamics of Integrin:Ligand Recognition. Returning to integrin:ligand interactions, we note that a pattern of competing desolvation and Coulombic stabilization effects was found in a recent computational study of the interactions of RGD peptides with a synthetic receptor (*71*). Indeed, a steered molecular dynamics simulation of the complex formed between the $\alpha v\beta 3$ integrin and a cyclic RGD peptide indicates that a single water molecule bridges the aspartate−MIDAS cation contact, serving as the gatekeeper to occlude solvent from the binding interface (*72*). Results from recent computational studies demonstrate that a cluster of nonpolar residues that surround the MIDAS region in the $\alpha L\beta 2$ integrin lowers the local dielectric constant (*61*) and enhances ligand binding mediated by glutamate−divalent cation electrostatic interactions (*73, 74*). Using PyMol to examine the residue distribution near its MIDAS Mg^{2+} in the $\alpha IIb\beta 3$ ectodomain:eptifibatide complex (PDB file 1TY6) (*14*), we observed a similar pattern of hydrophobic shielding. Thus, our observations on the role of entropy in stabilizing integrin:echistatin interactions have special interest in the context of current theoretical and experimental studies of the role of electrostatic and hydrophobic interactions in protein stability, ligand recognition, and structure-based drug design.

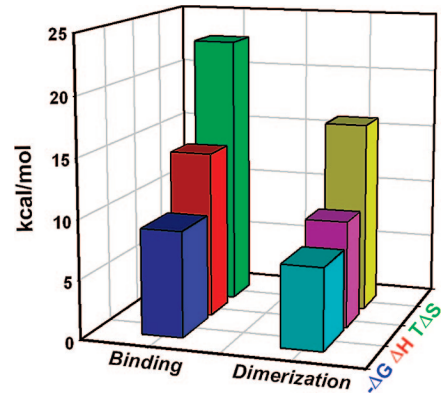

FIGURE 5: Thermodynamic parameters for echistatin binding and dimerization of the integrin:echistatin complex. This figure compares the equilibrium thermodynamic data obtained in this study for the formation of an $\alpha IIb\beta 3$:echistatin complex, as measured by SPR spectroscopy, with the corresponding parameters for dimerization of that complex, obtained by sedimentation equilibrium (*32*). The similar pattern of enthalpy/entropy compensation suggests desolvation processes contribute to both aspects of integrin:ligand interactions.

Transition-State Thermodynamics. Analysis of the temperature dependence of the rate constants for assembly and dissociation of the $\alpha IIb\beta 3$:echistatin complex by the transition-state theory indicates that electrostatic interactions may also govern the formation of its encounter complex. As illustrated in Figure 4, a substantial enthalpy barrier, $\Delta H_a^{\circ\ddagger} \sim 9$ kcal/mol, and a smaller entropy barrier, $T\Delta S_a^{\circ\ddagger} \sim -4$ kcal/mol, must be overcome on the path to product formation. Precedent for intermediates characterized by a large activation enthalpy/small activation entropy comes from lysozyme:antibody (*75*) and barnase:barstar complexes (*76*). Other investigators have demonstrated that for diffusion-limited protein:protein interactions, electrostatic interactions affect k_{on} but not k_{off} (*77*). Here, we note that the rate constant for the dissociation of the integrin:echistatin complex was nearly temperature-invariant, yielding $\Delta H_d^{\circ\ddagger}$ nearly zero. Thus, our observations appear consistent with a picture of a transition state with most of the electrostatic interactions that stabilize the receptor:ligand complex already in place but one in which desolvation of the binding interface is still incomplete (*78*).

Dimerization Thermodynamics. A comparison of the equilibrium thermodynamic parameters for assembly of the integrin:echistatin complex, determined in this study by SPR spectroscopy, to the analogous terms for ligand-induced receptor dimerization, derived from sedimentation equilibrium data that we collected as a function of the temperature (*32*), reveals a remarkably similar pattern of enthalpy/entropy compensation (Figure 5). This correspondence suggests that the initial binding event, which is required for integrin dimerization at temperatures below 40 °C (*32*), may well be the critical step that governs the overall favorable free energy of dimerization of the $\alpha IIb\beta 3$:rEch complex. Conversely, because binding takes place in minutes, whereas dimerization requires hours, both steps may exhibit similar thermodynamics because desolvation entropy, initially of ion pairs and subsequently of transmembrane segments, is at work (*38, 79*).

ACKNOWLEDGMENT

Thanks to Eric D. Roush, Ph.D., Application Scientist, Southeastern U.S., Biacore, Inc.−GE Healthcare, for expert

advice on SPR experimental design, to Karen Buchmueller, Department of Chemistry, Wake Forest University, for expert advice on isothermal titration calorimetry, and to Fred Salsbury, Ph.D., Department of Physics, Wake Forest University, for helpful discussions on protein electrostatics. Thanks to Julie Edelson, Ph.D., for her editorial insights.

SUPPORTING INFORMATION AVAILABLE

SPR traces (RU versus time) obtained for αIIbβ3 binding to immobilized RGDF-rEch as a function of the temperature from 15 to 40 °C, also including fitted lines and residuals plots and an accompanying legend (Supplementary Figure 1). This material is available free of charge via the Internet at http://pubs.acs.org.

REFERENCES

1. Hynes, R. O. (2002) Integrins: Bidirectional, allosteric signaling machines. *Cell 110*, 673–687.
2. Ruggeri, Z. M. (2002) Platelets in atherothrombosis. *Nat. Med. 8*, 1227–1234.
3. Ginsberg, M. H., Partridge, A., and Shattil, S. J. (2005) Integrin regulation. *Curr. Opin. Cell Biol. 17*, 509–516.
4. Shattil, S. J., and Newman, P. J. (2004) Integrins: Dynamic scaffolds for adhesion and signaling in platelets. *Blood 104*, 1606–1615.
5. Weisel, J. W. (2005) Fibrinogen and fibrin. *Adv. Protein Chem. 70*, 247–299.
6. Parise, L. V. (1999) Integrin αIIbβ3 signaling in platelet adhesion and aggregation. *Curr. Opin. Cell Biol. 11*, 597–601.
7. Leisner, T. M., Yuan, W., DeNofrio, J. C., Liu, J., and Parise, L. V. (2007) Tickling the tails: Cytoplasmic domain proteins that regulate integrin αIIbβ3 activation. *Curr. Opin. Hematol. 14*, 255–261.
8. Ma, Y. Q., Yang, J., Pesho, M. M., Vinogradova, O., Qin, J., and Plow, E. F. (2006) Regulation of integrin αIIbβ3 activation by distinct regions of its cytoplasmic tails. *Biochemistry 45*, 6656–6662.
9. Travis, M. A., Humphries, J. D., and Humphries, M. J. (2003) An unraveling tale of how integrins are activated from within. *Trends Pharmacol. Sci. 24*, 192–197.
10. Liddington, R. C., and Ginsberg, M. H. (2002) Integrin activation takes shape. *J. Cell Biol. 158*, 833–839.
11. Ratnikov, B. I., Partridge, A. W., and Ginsberg, M. H. (2005) Integrin activation by talin. *J. Thromb. Haemostasis 3*, 1783–1790.
12. Xiong, J. P., Stehle, T., Diefenbach, B., Zhang, R., Dunker, R., Scott, D. L., Joachimiak, A., Goodman, S. L., and Arnaout, M. A. (2001) Crystal structure of the extracellular segment of integrin αvβ3. *Science 294*, 339–345.
13. Xiong, J. P., Stehle, T., Zhang, R., Joachimiak, A., Frech, M., Goodman, S. L., and Arnaout, M. A. (2002) Crystal structure of the extracellular segment of integrin αvβ3 in complex with an Arg-Gly-Asp ligand. *Science 296*, 151–155.
14. Xiao, T., Takagi, J., Coller, B. S., Wang, J. H., and Springer, T. A. (2004) Structural basis for allostery in integrins and binding to fibrinogen-mimetic therapeutics. *Nature 432*, 59–67.
15. Weisel, J. W., Nagaswami, C., Vilaire, G., and Bennett, J. S. (1992) Examination of the platelet membrane glycoprotein IIb−IIIa complex and its interaction with fibrinogen and other ligands by electron microscopy. *J. Biol. Chem. 267*, 16637–16643.
16. Du, X., Gu, M., Weisel, J. W., Nagaswami, C., Bennett, J. S., Bowditch, R., and Ginsberg, M. H. (1993) Long range propagation of conformational changes in integrin $\alpha_{IIb}\beta_3$. *J. Biol. Chem. 268*, 23087–23092.
17. Hussain, M. A., and Siedlecki, C. A. (2004) The platelet integrin αIIbβ3 imaged by atomic force microscopy on model surfaces. *Micron 35*, 565–573.
18. Litvinov, R. I., Nagaswami, C., Vilaire, G., Shuman, H., Bennett, J. S., and Weisel, J. W. (2004) Functional and structural correlations of individual αIIbβ3 molecules. *Blood 104*, 3979–3985.
19. Adair, B. D., Xiong, J. P., Maddock, C., Goodman, S. L., Arnaout, M. A., and Yeager, M. (2005) Three-dimensional EM structure of the ectodomain of integrin αvβ3 in a complex with fibronectin. *J. Cell Biol. 168*, 1109–1118.
20. Hussain, M. A., Agnihotri, A., and Siedlecki, C. A. (2005) AFM imaging of ligand binding to platelet integrin αIIbβ3 receptors reconstituted into planar lipid bilayers. *Langmuir 21*, 6979–6986.
21. Luo, B. H., and Springer, T. A. (2006) Integrin structures and conformational signaling. *Curr. Opin. Cell Biol. 18*, 579–586.
22. Arnaout, M. A., Mahalingam, B., and Xiong, J. P. (2005) Integrin structure, allostery, and bidirectional signaling. *Annu. Rev. Cell Dev. Biol. 21*, 381–410.
23. Qin, J., Vinogradova, O., and Plow, E. F. (2004) Integrin bidirectional signaling: A molecular view. *PLoS Biol. 2*, e169.
24. Mould, A. P., and Humphries, M. J. (2004) Regulation of integrin function through conformational complexity: Not simply a knee-jerk reaction? *Curr. Opin. Cell Biol. 16*, 544–551.
25. Calvete, J. J., Marcinkiewicz, C., Monleon, D., Esteve, V., Celda, B., Juarez, P., and Sanz, L. (2005) Snake venom disintegrins: Evolution of structure and function. *Toxicon 45*, 1063–1074.
26. Wijeyewickrema, L. C., Berndt, M. C., and Andrews, R. K. (2005) Snake venom probes of platelet adhesion receptors and their ligands. *Toxicon 45*, 1051–1061.
27. Gan, Z. R., Gould, R. J., Jacobs, J. W., Friedman, P. A., and Polokoff, M. A. (1988) Echistatin. A potent platelet aggregation inhibitor from the venom of the viper, *Echis carinatus*. *J. Biol. Chem. 263*, 19827–19832.
28. Wierzbicka-Patynowski, I., Niewiarowski, S., Marcinkiewicz, C., Calvete, J. J., Marcinkiewicz, M. M., and McLane, M. A. (1999) Structural requirements of echistatin for the recognition of αvβ3 and α5β1 integrins. *J. Biol. Chem. 274*, 37809–37814.
29. Hantgan, R. R., Stahle, M. C., Connor, J. H., Connor, R. F., and Mousa, S. A. (2007) αIIbβ3 priming and clustering by orally active and intravenous integrin antagonists. *J. Thromb. Haemostasis 5*, 542–550.
30. Mousa, S. A., Bozarth, J. M., Naik, U. P., and Slee, A. (2001) Platelet GPIIb/IIIa binding characteristics of small molecule RGD mimetic: Distinct binding profile for roxifiban. *Br. J. Pharmacol. 133*, 331–336.
31. Bassler, N., Loeffler, C., Mangin, P., Yuan, Y., Schwarz, M., Hagemeyer, C. E., Eisenhardt, S. U., Ahrens, I., Bode, C., Jackson, S. P., and Peter, K. (2006) A mechanistic model for paradoxical platelet activation by ligand-mimetic αIIbβ3 (GPIIb/IIIa) antagonists. *Arterioscler., Thromb., Vasc. Biol. 27*, e9–15.
32. Hantgan, R. R., Stahle, M. C., Connor, J. H., Lyles, D. S., Horita, D. A., Rocco, M., Nagaswami, C., Weisel, J. W., and McLane, M. A. (2004) The disintegrin echistatin stabilizes integrin αIIbβ3's open conformation and promotes its oligomerization. *J. Mol. Biol. 342*, 1625–1636.
33. Hantgan, R. R., Stahle, M. C., Connor, J. H., Horita, D. A., Rocco, M., McLane, M. A., Yakovlev, S., and Medved, L. V. (2006) Integrin αIIbβ3:ligand interactions are linked to binding-site remodeling. *Protein Sci. 15*, 1893–1906.
34. Schuck, P. (1997) Use of surface plasmon resonance to probe the equilibrium and dynamic aspects of interactions between biological macromolecules. *Annu. Rev. Biophys. Biomol. Struct. 26*, 541–566.
35. Baird, C. L., and Myszka, D. G. (2001) Current and emerging commercial optical biosensors. *J. Mol. Recognit. 14*, 261–268.
36. Hantgan, R. R., Braaten, J. V., and Rocco, M. (1993) Dynamic light scattering studies of $\alpha_{IIb}\beta_3$ solution conformation. *Biochemistry 32*, 3935–3941.
37. Hantgan, R. R., Paumi, C, Rocco, M., and Weisel, J. W. (1999) Effects of ligand-mimetic peptides Arg-Gly-Asp-X (X = Phe, Trp, Ser) on αIIbβ3 integrin conformation and oligomerization. *Biochemistry 38*, 14461–14464.
38. Hantgan, R. R., Lyles, D. S., Mallett, T. C., Rocco, M., Nagaswami, C., and Weisel, J. W. (2003) Ligand binding promotes the entropy-driven oligomerization of integrin αIIbβ3. *J. Biol. Chem. 278*, 3417–3426.
39. Day, Y. S., Baird, C. L., Rich, R. L., and Myszka, D. G. (2002) Direct comparison of binding equilibrium, thermodynamic, and rate constants determined by surface- and solution-based biophysical methods. *Protein Sci. 11*, 1017–1025.
40. Schuck, P., and Minton, A. P. (1996) Analysis of mass transport-limited binding kinetics in evanescent wave biosensors. *Anal. Biochem. 240*, 262–272.
41. Myszka, D. G., He, X., Dembo, M., Morton, T. A., and Goldstein, B. (1998) Extending the range of rate constants available from BIACORE: Interpreting mass transport-influenced binding data. *Biophys. J. 75*, 583–594.

42. Leavitt, S., and Freire, E. (2001) Direct measurement of protein binding energetics by isothermal titration calorimetry. *Curr. Opin. Struct. Biol. 11*, 560–566.
43. Opatowski, E., Kozlov, M. M., and Lichtenberg, D. (1973) Partitioning of octyl glucoside between octyl glucoside/phosphatidylcholine mixed aggregates and aqueous media as studied by isothermal titration calorimetry. *Biophys. J. 73*, 1448–1457.
44. Winzor, D. J., and Jackson, C. M. (2005) Interpretation of the temperature dependence of rate constants in biosensor studies. *Anal. Biochem. 337*, 289–293.
45. Winzor, D. J., and Jackson, C. M. (2006) Interpretation of the temperature dependence of equilibrium and rate constants. *J. Mol. Recognit. 19*, 389–407.
46. McLane, M. A., Vijay-Kumar, S., Marcinkiewicz, C., Calvete, J. J., and Niewiarowski, S. (1996) Importance of the structure of the RGD-containing loop in the disintegrins echistatin and eristostatin for recognition of αIIbβ3 and αvβ3 integrins. *FEBS Lett. 391*, 139–143.
47. Gilli, P., Ferretti, V., and Gilli, G. (1994) Enthalpy−entropy compensation in drug−receptor binding. *J. Phys. Chem. 98*, 1515–1518.
48. Houk, K. N., Leach, A. G., Kim, S. P., and Zhang, X. (2003) Binding affinities of host−guest, protein−ligand, and protein−transition-state complexes. *Angew. Chem., Int. Ed. 42*, 4872–4897.
49. Cook, J. J., Bednar, B., Lynch, J., Gould, R. J., Egbertson, M. S., Halczenko, W., Duggan, M. E., Hartman, G. D., Lo, M.-W., Murphy, G. M., Deckelbaum, L. I., Sax, F. L., and Barr, E. (1999) Tirofiban (Aggrastat). *Cardiovasc. Drug Rev. 17*, 199–224.
50. Scarborough, R. M., Rose, J. W., Naughton, M. A., Phillips, D. R., Nannizzi, L., Arfsten, A., Campbell, A. M., and Charo, I. F. (1993) Characterization of the integrin specificities of disintegrins isolated from American pit viper venoms. *J. Biol. Chem. 268*, 1058–1065.
51. Williams, D. H., Stephens, E., O'Brien, D. P., and Zhou, M. (2004) Understanding noncovalent interactions: Ligand binding energy and catalytic efficiency from ligand-induced reductions in motion within receptors and enzymes. *Angew. Chem., Int. Ed. 43*, 6596–6616.
52. Klebe, G., and Bohm, H. J. (1997) Energetic and entropic factors determining binding affinity in protein−ligand complexes. *J. Recept. Signal Transduction Res. 17*, 459–473.
53. Chandler, D. (2005) Interfaces and the driving force of hydrophobic assembly. *Nature 437*, 640–647.
54. Dill, K. A., and Bromberg, S. (2003) Water, in *Molecular Driving Forces. Statistical Thermdynamics in Chemistry and Biology*, pp 563–591, Garland Science, New York.
55. Stites, W. E. (1997) Protein−protein interactions: Interface structure, binding thermodynamics, and mutational analysis. *Chem. Rev. 97*, 1233–1250.
56. Kauzmann, W. (1959) Some factors in the intrepretation of protein denaturation. *Adv. Protein Chem. 14*, 1–63.
57. Tanford, C. (1997) How protein chemists learned about the hydrophobic factor. *Protein Sci. 6*, 1358–1366.
58. Marcus, Y. (2007) Solvent release upon ion association from entropy data. II. *J. Phys. Chem. B 111*, 572–580.
59. Thomas, A. S., and Elcock, A. H. (2004) Molecular simulations suggest protein salt bridges are uniquely suited to life at high temperatures. *J. Am. Chem. Soc. 126*, 2208–2214.
60. Barril, X., Aleman, C., Orozco, M., and Luque, F. J. (1998) Salt bridge interactions: Stability of the ionic and neutral complexes in the gas phase, in solution, and in proteins. *Proteins 32*, 67–79.
61. Dudev, T., and Lim, C. (2003) Principles governing Mg, Ca, and Zn binding and selectivity in proteins. *Chem. Rev. 103*, 773–788.
62. Dominy, B. N., Minoux, H., and Brooks, C. L., III (2004) An electrostatic basis for the stability of thermophilic proteins. *Proteins 57*, 128–141.
63. Prorok, M., and Castellino, F. J. (1998) Thermodynamics of binding of calcium, magnesium, and zinc to the *N*-methyl-D-aspartate receptor ion channel peptidic inhibitors, conantokin-G and conantokin-T. *J. Biol. Chem. 273*, 19573–19578.
64. Shiroishi, M., Yokota, A., Tsumoto, K., Kondo, H., Nishimiya, Y., Horii, K., Matsushima, M., Ogasahara, K., Yutani, K., and Kumagai, I. (2001) Structural evidence for entropic contribution of salt bridge formation to a protein antigen−antibody interaction: The case of hen lysozyme−HyHEL-10 Fv complex. *J. Biol. Chem. 276*, 23042–23050.
65. Dekker, F. J., de Mol, N. J., Bultinck, P., Kemmink, J., Hilbers, H. W., and Liskamp, R. M. (2003) Role of solution conformation and flexibility of short peptide ligands that bind to the p56(lck) SH2 domain. *Bioorg. Med. Chem. 11*, 941–949.
66. de Mol, N. J., Dekker, F. J., Broutin, I., Fischer, M. J., and Liskamp, R. M. (2005) Surface plasmon resonance thermodynamic and kinetic analysis as a strategic tool in drug design. Distinct ways for phosphopeptides to plug into Src- and Grb2 SH2 domains. *J. Med. Chem. 48*, 753–763.
67. Deinum, J., Gustavsson, L., Gyzander, E., Kullman-Magnusson, M., Edstrom, A., and Karlsson, R. (2002) A thermodynamic characterization of the binding of thrombin inhibitors to human thrombin, combining biosensor technology, stopped-flow spectrophotometry, and microcalorimetry. *Anal. Biochem. 300*, 152–162.
68. Dell'Orco, D., Xue, W. F., Thulin, E., and Linse, S. (2005) Electrostatic contributions to the kinetics and thermodynamics of protein assembly. *Biophys. J. 88*, 1991–2002.
69. Shiroishi, M., Kuroki, K., Tsumoto, K., Yokota, A., Sasaki, T., Amano, K., Shimojima, T., Shirakihara, Y., Rasubala, L., van der Merwe, P. A., Kumagai, I., Kohda, D., and Maenaka, K. (2006) Entropically driven MHC class I recognition by human inhibitory receptor leukocyte Ig-like receptor B1 (LILRB1/ILT2/CD85j). *J. Mol. Biol. 355*, 237–248.
70. Moll, D., Schweinsberg, S., Hammann, C., and Herberg, F. W. (2007) Comparative thermodynamic analysis of cyclic nucleotide binding to protein kinase A. *Biol. Chem. 388*, 163–172.
71. Chen, W., Chang, C. E., and Gilson, M. K. (2006) Concepts in receptor optimization: Targeting the RGD peptide. *J. Am. Chem. Soc. 128*, 4675–4684.
72. Craig, D., Gao, M., Schulten, K., and Vogel, V. (2004) Structural insights into how the MIDAS ion stabilizes integrin binding to an RGD peptide under force. *Structure 12*, 2049–2058.
73. San, S. E., Mercero, J. M., Stote, R. H., Dejaegere, A., Cossio, F. P., and Lopez, X. (2006) On the affinity regulation of the metal-ion-dependent adhesion sites in integrins. *J. Am. Chem. Soc. 128*, 3554–3563.
74. Song, G., Yang, Y., Liu, J. H., Casasnovas, J. M., Shimaoka, M., Springer, T. A., and Wang, J. H. (2005) An atomic resolution view of ICAM recognition in a complex between the binding domains of ICAM-3 and integrin αIIbβ3. *Proc. Natl. Acad. Sci. U.S.A. 102*, 366–371.
75. Xavier, K. A., and Willson, R. C. (1998) Association and dissociation kinetics of anti-hen egg lysozyme monoclonal antibodies HyHEL-5 and HyHEL-10. *Biophys. J. 74*, 2036–2045.
76. Frisch, C., Fersht, A. R., and Schreiber, G. (2001) Experimental assignment of the structure of the transition state for the association of barnase and barstar. *J. Mol. Biol. 308*, 69–77.
77. Selzer, T., Albeck, S., and Schreiber, G. (2000) Rational design of faster associating and tighter binding protein complexes. *Nat. Struct. Biol. 7*, 537–541.
78. Schreiber, G. (2002) Kinetic studies of protein−protein interactions. *Curr. Opin. Struct. Biol. 12*, 41–47.
79. Zhang, J., and Lazaridis, T. (2006) Calculating the free energy of association of transmembrane helices. *Biophys. J. 91*, 1710–1723.

BI701877A